Paper 96

Proceedings of the Eleventh International Conference
on Computational Structures Technology,
B.H.V. Topping, (Editor),
Civil-Comp Press, Stirlingshire, Scotland

Computation of Eigenvalues for Thick and Thin Circular and Annular Plates using a Unified Ritz-Based Formulation

L. Dozio
Department of Aerospace Engineering
Politecnico di Milano, Milan, Italy

Abstract

This paper presents a novel unified Ritz-based method for reliable computation of eigenvalues of both thick and thin, circular and annular plates with different boundary conditions. The solution is based on an appropriate and simple formulation capable of handling in an unified way a large variety of two-dimensional higher-order plate theories. The formulation is also invariant with respect to the set of Ritz admissible functions. In this work, accurate upper-bound vibration solutions are presented by using kinematic models up to sixth order and products of Chebyshev polynomials and boundary-compliant functions. Considering the circumferential symmetry of circular plates and the two-dimensional nature of underlying theories, the present method is also computationally efficient since only single series of trial functions in the radial direction are required.

Keywords: free vibration, circular and annular plates, higher-order plate theories, variable-kinematic Ritz method.

1 Introduction

When dealing with vibration analysis of plate-like structures, one is typically faced with the problem of selecting the best structural model which yields system eigenvalues with desired accuracy and acceptable computational burden. Modeling approaches range from fully three-dimensional (3-D) models, without any simplifying assumption on the kinematics of deformation, to traditional plate theories, like classical plate theory (CPT) and first-order shear deformation theory (FSDT), based on a reduction of the 3-D problem to simple and economical two-dimensional (2-D) models [1].

Many attempts lying in the middle have appeared in the recent literature. They fall into the category of so-called refined or higher-order plate theories, where the conventional kinematics of FSDT is enriched with various higher-order terms as power series expansion of the thickness coordinate [2, 3, 4, 5, 6, 7, 8]. The aim of such refined theories is to preserve the 2-D nature of the model and thus avoid the complexity and computational inefficiency of 3-D elasticity solutions, while improving, compared to classical theories, the capabilities of estimating the correct mechanical behavior especially when thickness-to-length ratio of the plate increases, accurate through-the-thickness distribution of displacements and stresses is sought and discrete high frequency analysis is required.

In contrast to CPT and FSDT, higher-order theories typically lead to complex mathematical formulations of the structural problem. Derivation and computer implementation of the corresponding models would be less cumbersome with the availability of appropriate techniques capable of handling in an easy and efficient way arbitrary refinements of classical theories. Furthermore, it would be highly desirable to rely on an unified modeling framework giving the ability of performing comparisons of different theories of increasing complexity without the need of a new modeling effort each time.

A unified Ritz-based formulation based on an entire class of 2-D higher-order theories is presented here to accurately compute eigenvalues of thick and thin isotropic circular and annular plates with arbitrary boundary conditions. Several studies have been devoted to free vibration analysis of circular and annular plates. Most of them presented the natural frequencies on the basis of CPT and FSDT (see, e.g., [9, 10, 11, 12, 13]). A satisfactory number of papers appeared in the literature that carried out a 3-D vibration analysis [14, 15, 16, 17, 18]. However, higher-order plate theories were employed only in few works [19, 20, 21]. As reported by So and Leissa in their paper [15]: " [...] *besides the 2-D Mindlin theory used here for comparison [...], there are higher order 2-D plate theories proposed by numerous authors. Their governing equations are much more complicated than those of the Mindlin theory. One wonders how accurate their frequencies would be in representing a 3-D problem* [...] ". One goal of this study is to contribute in providing an answer to the above question.

As a further remark, all previous works on free vibration of circular and annular plates modeled according to 2-D theories suffer from a common shortcoming: they rely on axiomatic models with a fixed kinematic theory. As a result, the development of a refined theory of a certain order requires each time a new mathematical effort along with the related code implementation. This process can be cumbersome and prone to errors. The powerful yet simple method presented in this study overcomes the above deficiency.

The present formulation can be considered as an extension to circular plates of the variable-kinematic Ritz method developed in [22], which was focused on straight-sided quadrilateral plates. The formulation is invariant with respect to both the specific plate theory and the set of admissible functions. In other words, a unified modeling framework is derived in terms of simple modeling kernels, called *Ritz fundamental nuclei*, which are properly expanded to yield the mass and stiffness matrices of the model. In this work, products of Chebyshev polynomials and boundary-compliant

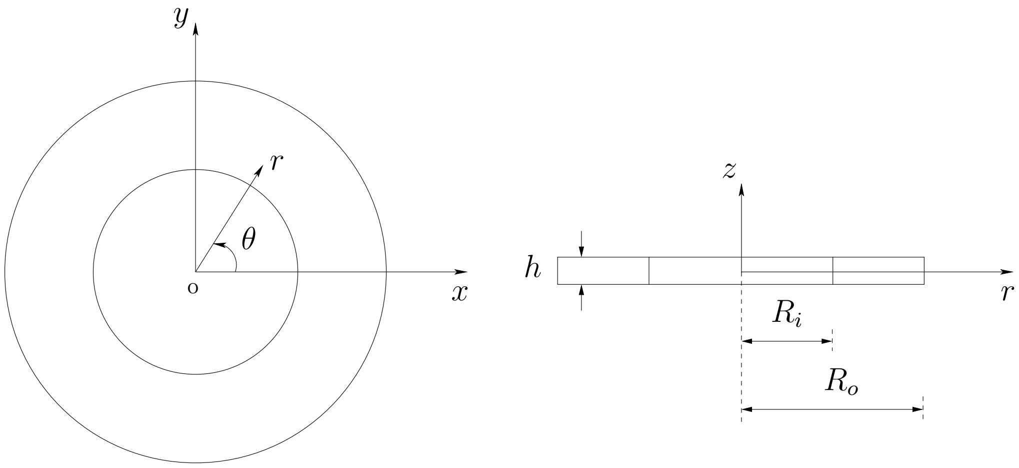

Figure 1: Geometry of an annular plate.

functions are chosen as Ritz trial set. Upper-bound vibration solutions based on different 2-D models are shown and compared with various thin and thick cases available in the literature.

Considering the circumferential symmetry of circular plates and the 2-D nature of underlying theories, the present method is computationally efficient since only single series of trial functions in the radial direction are required. In addition, relying on a global approximation, the method has a high spectral accuracy and converges faster than local methods such as finite elements. As a result, the formulation derived in this work is accurate in providing benchmark values yet efficient to be used for design purposes and parametric analysis.

2 Theoretical formulation

An annular isotropic plate of outer radius R_o and inner radius R_i is considered as shown in Figure 1. The plate has uniform thickness h. An orthogonal cylindrical coordinate system is defined with radial direction r ($R_i \leq r \leq R_o$), circumferential direction θ ($0 \leq \theta \leq 2\pi$) and thickness direction z ($-h/2 \leq z \leq h/2$).

For generality and convenience, the present formulation is derived using a dimensionless coordinate ξ ($-1 \leq \xi \leq 1$) for the radial direction defined as follows

$$\xi = \frac{r}{\gamma} - \delta \tag{1}$$

where

$$\gamma = \frac{R_o - R_i}{2} \tag{2}$$

$$\delta = \frac{R_o + R_i}{R_o - R_i} \tag{3}$$

The displacement vector $\mathbf{u} = \mathbf{u}(\xi, \theta, z, t)$ of a generic point of the plate is given by

$$\mathbf{u}(\xi, \theta, z, t) = \begin{Bmatrix} u_\xi(\xi, \theta, z, t) \\ u_\theta(\xi, \theta, z, t) \\ u_z(\xi, \theta, z, t) \end{Bmatrix} \tag{4}$$

Strain components can be grouped into an in-plane strain vector $\boldsymbol{\varepsilon}_{\mathrm{p}}$ and out-of-plane (normal) strain vector $\boldsymbol{\varepsilon}_{\mathrm{n}}$ as follows

$$\boldsymbol{\varepsilon}_{\mathrm{p}} = \begin{Bmatrix} \varepsilon_{\xi\xi} \\ \varepsilon_{\theta\theta} \\ \gamma_{\xi\theta} \end{Bmatrix} \qquad \boldsymbol{\varepsilon}_{\mathrm{n}} = \begin{Bmatrix} \gamma_{\xi z} \\ \gamma_{\theta z} \\ \varepsilon_{zz} \end{Bmatrix} \tag{5}$$

Within the framework of linear, small strain, elasticity theory, strain vectors are related to displacements through the following equations

$$\boldsymbol{\varepsilon}_{\mathrm{p}} = \boldsymbol{D}_{\mathrm{p}}\mathbf{u} \tag{6}$$

$$\boldsymbol{\varepsilon}_{\mathrm{n}} = \boldsymbol{D}_{\mathrm{n}}\mathbf{u} + \boldsymbol{D}_z\mathbf{u} \tag{7}$$

where

$$\boldsymbol{D}_{\mathrm{p}} = \begin{bmatrix} \left(\dfrac{1}{\gamma}\right)\dfrac{\partial}{\partial \xi} & 0 & 0 \\[2ex] \left(\dfrac{1}{\gamma}\right)\dfrac{1}{\xi+\delta} & \left(\dfrac{1}{\gamma}\right)\dfrac{1}{\xi+\delta}\dfrac{\partial}{\partial \theta} & 0 \\[2ex] \left(\dfrac{1}{\gamma}\right)\dfrac{1}{\xi+\delta}\dfrac{\partial}{\partial \theta} & \left(\dfrac{1}{\gamma}\right)\left[\dfrac{\partial}{\partial \xi} - \dfrac{1}{\xi+\delta}\right] & 0 \end{bmatrix} \tag{8}$$

$$\boldsymbol{D}_{\mathrm{n}} = \begin{bmatrix} 0 & 0 & \left(\dfrac{1}{\gamma}\right)\dfrac{\partial}{\partial \xi} \\[2ex] 0 & 0 & \left(\dfrac{1}{\gamma}\right)\dfrac{1}{\xi+\delta}\dfrac{\partial}{\partial \theta} \\[2ex] 0 & 0 & 0 \end{bmatrix} \tag{9}$$

and

$$\boldsymbol{D}_z = \mathrm{diag}\left[\frac{\partial}{\partial z}\right] \tag{10}$$

Accordingly, the stress vector can be partitioned into in-plane $\boldsymbol{\sigma}_{\mathrm{p}}$ and out-of-plane $\boldsymbol{\sigma}_{\mathrm{n}}$ components. Using Eqs. (6) and (7), the three-dimensional Hooke's law can be written as

$$\begin{aligned} \boldsymbol{\sigma}_{\mathrm{p}} &= \mathbf{C}_{\mathrm{pp}}\boldsymbol{D}_{\mathrm{p}}\mathbf{u} + \mathbf{C}_{\mathrm{pn}}\boldsymbol{D}_{\mathrm{n}}\mathbf{u} + \mathbf{C}_{\mathrm{pn}}\boldsymbol{D}_z\mathbf{u} \\ \boldsymbol{\sigma}_{\mathrm{n}} &= \mathbf{C}_{\mathrm{np}}\boldsymbol{D}_{\mathrm{p}}\mathbf{u} + \mathbf{C}_{\mathrm{nn}}\boldsymbol{D}_{\mathrm{n}}\mathbf{u} + \mathbf{C}_{\mathrm{nn}}\boldsymbol{D}_z\mathbf{u} \end{aligned} \tag{11}$$

where the following matrices of stiffness coefficients are introduced:

$$
\mathbf{C}_{\mathrm{pp}} = \begin{bmatrix} C_{11} & C_{12} & 0 \\ C_{12} & C_{22} & 0 \\ 0 & 0 & C_{66} \end{bmatrix}, \quad \mathbf{C}_{\mathrm{pn}} = \begin{bmatrix} 0 & 0 & C_{13} \\ 0 & 0 & C_{23} \\ 0 & 0 & 0 \end{bmatrix}
$$
$$
\mathbf{C}_{\mathrm{np}} = \begin{bmatrix} 0 & 0 & 0 \\ 0 & 0 & 0 \\ C_{13} & C_{23} & 0 \end{bmatrix}, \quad \mathbf{C}_{\mathrm{nn}} = \begin{bmatrix} C_{55} & 0 & 0 \\ 0 & C_{44} & 0 \\ 0 & 0 & C_{33} \end{bmatrix} \tag{12}
$$

In the case of isotropic materials, the elastic coefficients are given by

$$
\begin{aligned}
C_{11} = C_{22} = C_{33} &= \frac{E(1-\nu)}{(1+\nu)(1-2\nu)} \\
C_{12} = C_{13} = C_{23} &= \frac{E\nu}{(1+\nu)(1-2\nu)} \\
C_{44} = C_{55} = C_{66} = G &= \frac{E}{2(1+\nu)}
\end{aligned} \tag{13}
$$

in which E is the Young's modulus, ν is the Poisson's ratio, and G is the shear modulus.

According to the approach developed by Carrera [23], an entire class of two-dimensional higher-order plate theories can be compactly described through the following indicial notation:

$$
\mathbf{u}(\xi, \theta, z, t) = F_\tau(z)\mathbf{u}_\tau(\xi, \theta, t) \qquad (\tau = 0, 1, \ldots, N) \tag{14}
$$

where $\mathbf{u}_\tau(\xi, \theta, t)$ is the displacement vector containing the unknown kinematic variables related to the specific plate theory, τ is an integer index related to the order N of the theory and $F_\tau(z)$ are selected functions in the thickness direction. The summation convention on indices appearing twice is implied in Eq. (14). In this work, the z expansion is implemented via Taylor polynomials. For the sake of brevity, a higher-order theory of order N will be indicated in the following by HOT_N. For example, HOT_3 is a plate theory of order 3 based on the following assumed kinematic field:

$$
\begin{aligned}
u_\xi &= u_{\xi 0} + z u_{\xi 1} + z^2 u_{\xi 2} + z^3 u_{\xi 3} \\
u_\theta &= u_{\theta 0} + z u_{\theta 1} + z^2 u_{\theta 2} + z^3 u_{\theta 3} \\
u_z &= u_{z0} + z u_{z1} + z^2 u_{z2} + z^3 u_{z3}
\end{aligned}
$$

The total number of kinematic degrees of freedom for a given HOT_N is $3\,(N+1)$.

Assuming a harmonic motion and considering the circumferential symmetry of the plate about the coordinate θ, the displacements can be expressed as

$$
\mathbf{u}(\xi, \theta, z, t) = F_\tau(z) \left\{ \begin{array}{c} \hat{u}_{\xi\tau}(\xi)\cos(n\theta) \\ \hat{u}_{\theta\tau}(\xi)\sin(n\theta) \\ \hat{u}_{z\tau}(\xi)\cos(n\theta) \end{array} \right\} e^{j\omega t} \tag{15}
$$

Boundary condition	$f_{\xi\tau}^{\rm inn}$	$f_{\theta\tau}^{\rm inn}$	$f_{z\tau}^{\rm inn}$	$f_{\xi\tau}^{\rm out}$	$f_{\theta\tau}^{\rm out}$	$f_{z\tau}^{\rm out}$
Clamped	$1+\xi$	$1+\xi$	$1+\xi$	$1-\xi$	$1-\xi$	$1-\xi$
Simply-supported	1	$1+\xi$	$1+\xi$	1	$1-\xi$	$1-\xi$
Free	1	1	1	1	1	1

Table 1: Boundary functions.

or, in matrix form,

$$\mathbf{u}(\xi, \theta, z, t) = F_\tau(z)\mathbf{\Theta}(n\theta)\hat{\mathbf{u}}_\tau(\xi)e^{j\omega t} \tag{16}$$

where $\hat{u}$'s are amplitude functions of the dimensionless radial coordinate, $n = 0, 1, 2, \ldots$ is the circumferential wavenumber and $\mathbf{\Theta}(n\theta) = \mathrm{diag}(\cos n\theta, \sin n\theta, \cos n\theta)$. Note that $n = 0$ in Eq. (15) yields axisymmetric vibration which involves only u_ξ and u_z. A complementary displacement field can be also used by replacing $\cos(n\theta)$ by $\sin(n\theta)$, and conversely, in Eq. (15). In this case, torsional vibration modes are obtained when $n = 0$.

A standard Ritz solution is sought for each component of the displacement vector $\hat{\mathbf{u}}_\tau(\xi)$ as follows

$$\begin{aligned} \hat{u}_{\xi\tau}(\xi) &= \phi_{\xi\tau i}(\xi)c_{\xi\tau i} \\ \hat{u}_{\theta\tau}(\xi) &= \phi_{\theta\tau i}(\xi)c_{\theta\tau i} \qquad\qquad (i = 1, 2, \ldots, M) \\ \hat{u}_{z\tau}(\xi) &= \phi_{z\tau i}(\xi)c_{z\tau i} \end{aligned} \tag{17}$$

where M is the order of the Ritz expansion, $c_{\alpha\tau i}$ ($\alpha = \xi, \theta, z$) are the unknown Ritz coefficients, and $\phi_{\alpha\tau i}$ are the corresponding Ritz trial functions. Note that, as before for the theory-related index τ in Eq. (14), Ritz-related dummy index i in Eq. (17) implies summation. The i-th admissible function $\phi_{\alpha\tau i}(\xi)$ is chosen here as the product of boundary-compliant functions and the one-dimensional Chebyshev polynomial [17]:

$$\phi_{\alpha\tau i}(\xi) = f_{\alpha\tau}^{\rm inn}(\xi)f_{\alpha\tau}^{\rm out}(\xi)\cos\left[(i-1)\arccos(\xi)\right] \tag{18}$$

where $f_{\alpha\tau}^{\rm inn}(\xi)$ and $f_{\alpha\tau}^{\rm out}(\xi)$ enable the displacement component $u_{\alpha\tau}$ to satisfy the geometric boundary conditions at the inner ($\xi = -1$) and outer ($\xi = +1$) edges of the plate, respectively. The boundary functions corresponding to the most common boundary conditions are reported in Table 1. It is clear that $f_{\alpha\tau}^{\rm inn}(\xi) = 1$ in the case of a solid circular plate. Chebyshev polynomials form a complete and orthogonal set in the interval $[-1, +1]$. As such, good convergence and numerical stability of the method are expected.

For the sake of compact notation, Eq. (17) is rearranged in matrix form as follows

$$\hat{\mathbf{u}}_\tau(\xi) = \mathbf{\Phi}_{\tau i}(\xi)\mathbf{c}_{\tau i} \tag{19}$$

where $\mathbf{\Phi}_{\tau i}(\xi) = \mathrm{diag}(\phi_{\xi\tau i}, \phi_{\theta\tau i}, \phi_{z\tau i})$ and $\mathbf{c}_{\tau i} = \{c_{\xi\tau i} \quad c_{\theta\tau i} \quad c_{z\tau i}\}^T$. Therefore, the displacement vector in Eq. (16) is given by

$$\mathbf{u}(\xi, \theta, z, t) = F_\tau(z)\mathbf{\Theta}(n\theta)\mathbf{\Phi}_{\tau i}(\xi)\mathbf{c}_{\tau i}e^{j\omega t} \tag{20}$$

The potential and kinetic energy of the plate are expressed, respectively, as

$$U=\frac{1}{2}\gamma^2\int_{-1}^{+1}\int_{0}^{2\pi}\int_{-\frac{h}{2}}^{+\frac{h}{2}}\left(\boldsymbol{\varepsilon}_{\mathrm{p}}^T\mathbf{C}_{\mathrm{pp}}\boldsymbol{\varepsilon}_{\mathrm{p}}+\boldsymbol{\varepsilon}_{\mathrm{p}}^T\mathbf{C}_{\mathrm{pn}}\boldsymbol{\varepsilon}_{\mathrm{n}}+\boldsymbol{\varepsilon}_{\mathrm{n}}^T\mathbf{C}_{\mathrm{np}}\boldsymbol{\varepsilon}_{\mathrm{p}}+\boldsymbol{\varepsilon}_{\mathrm{n}}^T\mathbf{C}_{\mathrm{nn}}\boldsymbol{\varepsilon}_{\mathrm{n}}\right)(\xi+\delta)\,\mathrm{d}z\mathrm{d}\theta\mathrm{d}\xi \tag{21}$$

and

$$T=\frac{1}{2}\gamma^2\int_{-1}^{+1}\int_{0}^{2\pi}\int_{-\frac{h}{2}}^{+\frac{h}{2}}\rho\left[\left(\frac{\partial u_\xi}{\partial t}\right)^2+\left(\frac{\partial u_\theta}{\partial t}\right)^2+\left(\frac{\partial u_z}{\partial t}\right)^2\right](\xi+\delta)\mathrm{d}z\mathrm{d}\theta\mathrm{d}\xi \tag{22}$$

where ρ is the mass density of the plate. Substituting Eq. (20) into Eqs. (6) and (7) and using Hooke's law in Eq. (11), the expressions of the maximum potential and kinetic energy of the plate vibrating harmonically can be compactly written as follows:

$$U_{\max}=\frac{1}{2}\mathbf{c}_{\tau i}^T\mathbf{K}_{\tau sij}\mathbf{c}_{sj} \tag{23}$$

and

$$T_{\max}=\frac{1}{2}\omega^2\mathbf{c}_{\tau i}^T\mathbf{M}_{\tau sij}\mathbf{c}_{sj} \tag{24}$$

where s and j are other theory-related and Ritz-related dummy indices, respectively. In the above equations, when $n\neq 0$, $\mathbf{K}_{\tau sij}$ and $\mathbf{M}_{\tau sij}$ are 3×3 matrices given by

$$\begin{aligned}\mathbf{K}_{\tau sij}=\gamma^2\int_{-1}^{+1}\int_{0}^{2\pi}\Big\{&\left[\boldsymbol{D}_{\mathrm{p}}\boldsymbol{\Theta}(n\theta)\boldsymbol{\Phi}_{\tau i}(\xi)\right]^T\left[\mathbf{Z}_{\tau s}^{\mathrm{pp}}\boldsymbol{D}_{\mathrm{p}}+\mathbf{Z}_{\tau s}^{\mathrm{pn}}\boldsymbol{D}_{\mathrm{n}}\right.\\&\left.+\mathbf{Z}_{\tau s_{,z}}^{\mathrm{pn}}\right]\boldsymbol{\Theta}(n\theta)\boldsymbol{\Phi}_{sj}(\xi)+\left[\boldsymbol{D}_{\mathrm{n}}\boldsymbol{\Theta}(n\theta)\boldsymbol{\Phi}_{\tau i}(\xi)\right]^T\left[\mathbf{Z}_{\tau s}^{\mathrm{np}}\boldsymbol{D}_{\mathrm{p}}\right.\\&\left.+\mathbf{Z}_{\tau s}^{\mathrm{nn}}\boldsymbol{D}_{\mathrm{n}}+\mathbf{Z}_{\tau s_{,z}}^{\mathrm{nn}}\right]\boldsymbol{\Theta}(n\theta)\boldsymbol{\Phi}_{sj}(\xi)+\left[\boldsymbol{\Theta}(n\theta)\boldsymbol{\Phi}_{\tau i}(\xi)\right]^T\left[\mathbf{Z}_{\tau_{,z}s}^{\mathrm{np}}\boldsymbol{D}_{\mathrm{p}}\right.\\&\left.+\mathbf{Z}_{\tau_{,z}s}^{\mathrm{nn}}\boldsymbol{D}_{\mathrm{n}}+\mathbf{Z}_{\tau_{,z}s_{,z}}^{\mathrm{nn}}\right]\boldsymbol{\Theta}(n\theta)\boldsymbol{\Phi}_{sj}(\xi)\Big\}(\xi+\delta)\,\mathrm{d}\theta\mathrm{d}\xi\end{aligned} \tag{25}$$

and

$$\mathbf{M}_{\tau sij}=\gamma^2\int_{-1}^{+1}\int_{0}^{2\pi}\left[\boldsymbol{\Theta}(n\theta)\boldsymbol{\Phi}_{\tau i}(\xi)\right]^T\mathbf{Z}_{\tau s}^{\rho}\boldsymbol{\Theta}(n\theta)\boldsymbol{\Phi}_{sj}(\xi)\,(\xi+\delta)\,\mathrm{d}\theta\mathrm{d}\xi \tag{26}$$

where $\mathbf{Z}_{\tau s}^{\mathrm{pp}},\ldots,\mathbf{Z}_{\tau s}^{\rho}$ are matrices of thickness integrals whose expression is given in Appendix A. Matrices in Eqs. (25) and (26) represent modeling kernels and are called *Ritz fundamental nuclei* of the present formulation. Indeed, they are invariant with respect to both the underlying kinematic theory and the set of Ritz admissible functions. In the case of axisymmetric modes, the condition $n=0$ yields fundamental nuclei $\mathbf{K}_{\tau sij}$ and $\mathbf{M}_{\tau sij}$ of dimension 2×2 since only u_ξ and u_z are involved. In the case of torsional vibration, the fundamental nuclei reduce to scalar quantities. The elements of $\mathbf{K}_{\tau sij}$ and $\mathbf{M}_{\tau sij}$ are explicitly reported in Appendix B.

The stiffness and mass matrices of the plate are built from the above nuclei through an assembly-like procedure. The nuclei are first expanded to $3(N+1) \times 3(N+1)$ matrices by varying the theory-related indices τ and s from 0 to N. This expansion yields

$$\mathbf{K}_{ij} = \begin{bmatrix} \mathbf{K}_{00ij} & \mathbf{K}_{0rij} & \mathbf{K}_{0Nij} \\ \mathbf{K}_{r0ij} & \mathbf{K}_{rrij} & \mathbf{K}_{rNij} \\ \mathbf{K}_{N0ij} & \mathbf{K}_{Nrij} & \mathbf{K}_{NNij} \end{bmatrix} \tag{27}$$

$$\mathbf{M}_{ij} = \begin{bmatrix} \mathbf{M}_{00ij} & \mathbf{M}_{0rij} & \mathbf{M}_{0Nij} \\ \mathbf{M}_{r0ij} & \mathbf{M}_{rrij} & \mathbf{M}_{rNij} \\ \mathbf{M}_{N0ij} & \mathbf{M}_{Nrij} & \mathbf{M}_{NNij} \end{bmatrix} \tag{28}$$

where $r = 1, \ldots, N-1$. Then, the final matrices $\mathbf{K}$ and $\mathbf{M}$ of dimensions $3M(N+1) \times 3M(N+1)$ are generated accordingly through variation of Ritz-related indeces i and j in the above quantities $\mathbf{K}_{ij}$ and $\mathbf{M}_{ij}$ and by applying the same assembly operations adopted for the nuclei expansion.

The extremization of the energy functional $\Pi = U_{\max} - T_{\max}$ with respect to the coefficients $\mathbf{c}_{\tau i}$ yields the following generalized eigenvalue problem:

$$\left(\mathbf{K} - \omega^2 \mathbf{M}\right) \mathbf{c} = \mathbf{0} \tag{29}$$

where $\mathbf{c}$ is the vector containing the unknown coefficients $\mathbf{c}_{sj}$.

3 Convergence and stability analysis

The mathematically complete set of admissible functions in Eq. (18) yields upper-bound frequency values with increasing accuracy towards exact solutions as the number of terms M retained in the series of Eq. (19) increases. However, nothing can be said in advance with regard to the efficiency of the present method in terms of rate of convergence. Furthermore, possible numerical issues associated with ill-conditioned eigenvalue problems in Eq. (29) when an high number of terms are taken should be pointed out.

The convergence and numerical stability of the method are studied in this section with respect to a clamped solid circular plate ($R_o = R$) with various thickness-to-radius h/R ratios. Clamping boundary conditions have been selected since convergence of such solutions is expected to be slower than for other edge conditions, even for the lowest frequency parameters [15, 22]. This is mainly due to the difficulty of global trial function in approximating the actual displacement field near the fixed boundary. Three cases are considered corresponding to a thin plate ($h/R = 0.01$), a moderately thick plate ($h/R = 0.1$), and a very thick plate ($h/R = 0.5$). The first six non-dimensional frequencies $\lambda = \omega R^2 \sqrt{\rho h/D}$, where $D = Eh^3/12(1-\nu^2)$ is the plate bending stiffness, are listed in Table 2 for three different kinematic theories of increasing complexity. Numerical results are shown as functions of increasing value of order M for the Ritz expansion in the radial direction. Frequency values with superscripts a and t denote axisymmetric and torsional vibration modes, respectively, corresponding to $n = 0$.

Table 2: Convergence of the first six frequency parameters $\lambda = \omega R^2 \sqrt{\rho h / D}$ for solid clamped circular plates.

			Mode					
Theory	h/R	M	1	2	3	4	5	6
HOT_1	0.01	8	11.304^a	23.518	38.568	43.976^a	56.410	67.232
		10	11.304	23.518	38.568	43.976	56.409	67.229
		20	11.304	23.518	38.568	43.976	56.409	67.229
	0.1	8	11.000^a	22.324	35.625	40.354^a	50.625	59.557
		10	11.000	22.324	35.625	40.354	50.624	59.556
		20	11.000	22.324	35.625	40.354	50.624	59.556
	0.5	8	7.3607^a	12.364	13.720	15.705^t	17.387	19.102^a
		10	7.3607	12.364	13.720	15.705	17.387	19.102
		18	7.3607	12.364	13.720	15.705	17.387	19.102
HOT_2	0.01	8	10.259^a	21.345	35.006	39.916^a	51.201	61.022
		10	10.244	21.314	34.955	39.858	51.129	60.938
		20	10.222	21.269	34.881	39.773	51.019	60.808
		30	10.218	21.260	34.867	39.757	50.999	60.783
		40	10.217	21.257	34.862	39.752	50.992	60.775
	0.1	8	10.030^a	20.426	32.713	37.085^a	46.647	54.963
		10	10.019	20.404	32.679	37.048	46.602	54.912
		20	10.010	20.386	32.652	37.018	46.566	54.870
		30	10.010	20.386	32.652	37.018	46.565	54.869
	0.5	8	7.0527^a	11.955	13.684	15.705^t	16.864	18.548^a
		10	7.0525	11.955	13.684	15.705	16.864	18.547
		16	7.0525	11.955	13.684	15.705	16.864	18.547
		18	7.0525	11.955	13.684	15.705	16.864	18.547
HOT_6	0.01	8	10.258^a	21.343	35.003	39.912^a	51.194	61.013
		10	10.243	21.312	34.952	39.853	51.122	60.928
		20	10.222	21.267	34.877	39.768	51.012	60.798
		30	10.217	21.258	34.863	39.752	50.991	60.773
		40	10.216	21.255	34.858	39.747	50.984	60.765

Table 2 – *(continued on next page)*

Table 2 – *(continued)*

Theory	h/R	M	Mode 1	2	3	4	5	6
	0.1	8	9.9973^a	20.310	32.449	36.766^a	46.167	54.340
		10	9.9862	20.288	32.416	36.728	46.121	54.286
		20	9.9746	20.265	32.381	36.689	46.073	54.230
		30	9.9735	20.263	32.377	36.685	46.068	54.224
	0.5	8	6.8094^a	11.501	13.659	15.705^t	16.234	17.829^a
		10	6.8075	11.498	13.657	15.705	16.231	17.827
		16	6.8060	11.497	13.657	15.705	16.230	17.825
		18	6.8060	11.497	13.657	15.705	16.230	17.825

As expected, all the frequency parameters monotonically decrease with the increase in the number of admissible functions, regardless of the thickness-to-radius ratio and the order of the kinematic model.

For each thickness-to-radius ratio, the rate of convergence of the method is very similar for HOT_2 and HOT_6. Although corresponding results are not shown here due to brevity reasons, the same can be said for kinematic models of intermediate order. From Table 2, it can be seen that fewer terms are needed for the frequency values to converge when the thickness dimension becomes significant. Indeed, all the first six frequency parameters converged to five-digit upper-bound values with $M = 16$ in the case of $h/R = 0.5$. When thinner plates are considered, the same frequencies are of only three- or four-digit accuracy even when the order M raises up to 30. A more rapid convergence as the plate thickness ratio increases has been also observed in 3-D Ritz-based vibration studies [16]. Moreover, the substantial invariance of the convergence behavior with respect to the assumed kinematic theory was also found in a previous work on quadrilateral straight-sided plate [22].

By further comparing solutions based on HOT_2 with those based on HOT_6, it is noted that, except for the thin case ($h/R = 0.01$) and the results corresponding to torsional modes, all the natural frequencies converged to different values according to the adopted theory. As shown in the next section, the accuracy of the solution for moderately thick and very thick plates is largely affected by the underlying kinematic model. In the case of thin plates, frequency values computed by plate theories of increasing order are all very close to each other and completely consistent with results obtained from the classical 2-D Kirchhoff theory (see Table 2.1 in [9]).

Tabulated results corresponding to a first-order HOT_1 kinematic theory show that the rate of convergence of the method is very fast in that case, regardless of the thickness-to-radius ratio. All the frequency parameters converged to five-digit upper-bound values with $M = 10$. However, it is observed that convergent results are all significantly higher than those obtained with more refined theories. This behavior is due to a locking mechanism, known as thickness locking (TL), which occurs when the kinematic model exhibits a constant distribution of the transverse normal strain ε_{zz} [22]. Note that TL effects are more distinct for thin plates and slightly decrease with increasing thickness.

As far as the numerical stability of the method is concerned, it can be noticed that the ill-conditioning of the eigenvalue problem is avoided even when a high number M of terms is taken to compute the frequency solutions. It is shown that stable numerical analysis can still be carried out when $M = 40$. Numerical tests involving up to 100 terms in the radial direction have been performed without reaching the upper limit yet. Such immunity against ill-conditioned behavior can be of great importance in improving the accuracy of the eigenfrequencies of higher order.

As a final remark, it can be observed that, from an engineering point of view, well-converged values are attained with $M = 20$ in all cases.

Similar analysis has been carried out on annular plates having different R_o/R_i ratios. The computed results, not shown here for brevity, have confirmed the above outlined conclusions.

4 Comparison results

The variable-kinematic Ritz formulation derived in Section 2 is here validated against some reference solutions available in the literature. In particular, the following analysis is focused on comparing eigenfrequencies of different annular plates obtained on the basis of higher-order 2-D theories with those computed using a fully 3-D approach. Results are given in tabulated form, so that listed solutions may serve as benchmark values for future comparison.

The first analysis is referred to annular plates with $R_o = (10/3)R_i$ and $h/R_o = 0.2$. Three cases with different combinations of boundary conditions at the inner and outer edges are considered. The first six frequency parameters $\lambda = \omega R_o^2\sqrt{\rho h/D}$ are sorted in Table 3 as a result of the adoption of kinematic models of order 2, 4, and 6. Present Ritz-based solutions are computed with $M = 30$ and compared with those obtained from three-dimensional analysis using orthogonally generated polynomial functions [16] and Chebyshev polynomials [17]. Note that the missing term with both the inner and outer edges clamped is related to a torsional mode, which was not computed in Ref. [16]. It is clear from Table 3 that frequency values arising from 2-D models converge towards 3-D based accurate solutions reported in [17] as the order N of the underlying theory increases. The agreement is excellent when computations are performed using a kinematic model of order 6. The accuracy is slightly worse, but still very good, for models of lower order. This shows that, using the variable-kinematic formulation presented in this work, one can easily select the theory refinement needed to achieve a desired accuracy without any further development effort and without the complexity and computational inefficiency associated to 3-D models.

Table 3: Frequency parameters $\lambda = \omega R_o^2 \sqrt{\rho h/D}$ for the first eight modes of annular plates with $R_o = (10/3)R_i$, $h/R_o = 0.2$ and various boundary conditions.

		Mode					
BC	Method	1	2	3	4	5	6
FF	Present (HOT_2)	4.6393	7.9075	11.222	15.389	15.662	19.030
	Present (HOT_4)	4.6196	7.8939	11.143	15.187	15.661	18.826
	Present (HOT_6)	4.6195	7.8939	11.143	15.187	15.661	18.826
	3D-Ritz [16]	4.6198	7.8939	11.143	15.189	15.662	18.826
FC	Present (HOT_2)	10.553	16.323	26.210	37.101	38.249	39.627
	Present (HOT_4)	10.442	16.020	25.645	36.214	37.339	39.598
	Present (HOT_6)	10.438	16.013	25.634	36.197	37.313	39.592
	3D-Ritz [16]	10.448	16.026	25.650	36.220	37.346	39.602
	3D-Ritz [17]	10.437	16.012	25.632	36.194	37.309	39.591
CC	Present (HOT_2)	31.822	32.548	35.451	41.442	48.220	50.147
	Present (HOT_4)	30.741	31.473	34.371	40.271	48.220	48.745
	Present (HOT_6)	30.696	31.430	34.333	40.238	48.220	48.713
	3D-Ritz [16]	30.743	31.474	34.370	40.266	–	48.736
	3D-Ritz [17]	30.688	31.422	34.325	40.231	48.220	48.707

Note also that upper-bound results obtained by the present method using HOT_4 and HOT_6 are slightly lower than those obtained in [16] from a 3-D analysis. This is probably due to the relatively low number of Ritz terms taken in the radial and thickness directions in the 3-D case.

Table 4: Frequency parameters $\lambda = \omega R_o \sqrt{\rho/G}$ for the first four antisymmetric modes of completely free annular plates with $R_o = 2R_i$.

			Mode			
h/R_o	n	Method	1	2	3	4
0.4	0^a	Present (HOT_1)	1.470	9.106	9.983	16.631
		Present (HOT_3)	1.388	8.344	9.167	14.498
		Present (HOT_6)	1.388	8.321	9.127	14.133
		3D-Ritz [17]	1.388	8.321	9.127	14.133
		3D-Ritz [15]	1.388	8.321	9.127	14.133
	1	Present (HOT_3)	1.944	8.049	8.554	8.974
		Present (HOT_6)	1.943	8.039	8.534	8.945
		3D-Ritz [17]	1.943	8.039	8.534	8.945
		3D-Ritz [15]	1.943	8.039	8.534	8.945
	2	Present (HOT_3)	0.691	3.127	8.422	8.814
		Present (HOT_6)	0.691	3.123	8.400	8.793
		3D-Ritz [17]	0.691	3.123	8.400	8.793
		3D-Ritz [15]	0.691	3.123	8.400	8.793
	3	Present (HOT_3)	1.681	4.459	8.834	9.007
		Present (HOT_6)	1.680	4.450	8.808	8.986
		3D-Ritz [17]	1.680	4.450	8.808	8.986
		3D-Ritz [15]	1.680	4.450	8.808	8.986
1	0^a	Present (HOT_1)	2.102	7.177	10.903	14.104
		Present (HOT_3)	1.984	6.129	9.360	10.411
		Present (HOT_6)	1.984	5.775	8.329	9.355
		3D-Ritz [17]	1.984	5.772	8.258	9.084
		3D-Ritz [15]	1.984	5.772	8.258	9.084
	1	Present (HOT_3)	2.002	3.939	6.145	7.959
		Present (HOT_6)	1.999	3.930	5.842	7.719
		3D-Ritz [17]	1.999	3.930	5.839	7.706
		3D-Ritz [15]	1.999	3.930	5.839	7.706

Table 4 – *(continued on next page)*

Table 4 – *(continued)*

h/R_o	n	Method	Mode 1	2	3	4
	2	Present (HOT_3)	1.040	2.858	5.213	6.424
		Present (HOT_6)	1.039	2.846	5.173	6.160
		3D-Ritz [17]	1.039	2.846	5.172	6.157
		3D-Ritz [15]	1.039	2.846	5.172	6.157
	3	Present (HOT_3)	2.326	3.975	6.521	7.072
		Present (HOT_6)	2.320	3.947	6.393	6.808
		3D-Ritz [17]	2.320	3.946	6.392	6.805
		3D-Ritz [15]	2.320	3.946	6.392	6.805

Another illustrative example is referred to a completely free annular plate with $R_o/R_i = 2$ and two different thickness-to-outer-radius ratios, $h/R_o = 0.4$ and $h/R_o = 1$. The first four non-dimensional frequencies $\lambda = \omega R_o\sqrt{\rho/G}$ corresponding to antisymmetric modes are shown in Table 4 for circumferential wavenumber n ranging from 0 to 3. Present solutions, computed with $M = 30$ and based on kinematic theories of increasing order, are compared with the 3-D Ritz series solutions available in [17] and [15]. By looking at results corresponding to axisymmetric modes when $h/R_o = 0.4$, it is confirmed that HOT_1 suffer from thickness locking. Therefore, it must be used along with the enforcement of null normal transverse stress condition [22]. It can be also observed that, except for a few higher-order axisymmetric modes in the very thick case ($h/R_o = 1$), the frequency solutions obtained with a 2-D sixth-order theory are all in excellent agreement with those from a 3-D analysis. The accuracy of the lowest modes is still very good in the case of $h/R_o = 0.4$ when HOT_3 is adopted. However, it is seen that, when relatively high-order modes of very thick plates are of interest, a kinematic theory of high refinement is required.

5 Conclusions

A novel variable-kinematic Ritz formulation capable of handling in an unified way an entire class of 2-D higher-order kinematic theories for accurate vibration analysis of circular and annular plates of any thickness has been derived. The method relies on suitable expansion of invariant kernels of the mass and stiffness matrix. The invariance is to be intended with respect to both the order of the theory and the type of Ritz trial functions. Considering the circumferential symmetric of the problem under study, the present method is also computationally efficient.

Upper-bound frequency values have been presented using products of boundary-compliant functions and Chebyshev polynomials. It has been shown that the method exhibits good convergence properties and a high numerical stability. As expected, increasing accuracy towards 3-D values in terms of frequency parameters has been found with theory refinement. Further, kinematic plate models of lower order are more sensitive to thickness-to-radius ratio, whereas accuracy is substantially independent from plate thickness when a highly refined theory is adopted.

References

[1] K.M. Liew, Y. Xiang, S. Kitipornchai, “Research on thick plate vibration: a literature survey”, Journal of Sound and Vibration, 180, 163-176, 1995.

[2] K.H. Lo, R.M. Christensen, E.M. Wu, “A high-order theory of plate deformation - part 1: homogeneous plates”, Journal of Applied Mechanics, 44, 663-668, 1977.

[3] M. Levinson, “An accurate, simple theory of the statics and dynamics of elastic plates”, Mechanics Research Communications, 7, 343-350, 1980.

[4] T. Kant, “Numerical analysis of thick plates”, Computer Methods in Applied Mechanics and Engineering, 31, 1-18, 1982.

[5] J.N. Reddy, “A refined nonlinear theory of plates with transverse shear deformation”, International Journal of Solids and Structures, 20, 881-896, 1984.

[6] N.F. Hanna, A.W. Leissa, “A higher order shear deformation theory for the vibration of thick plates”, Journal of Sound and Vibration, 170, 545-555, 1994.

[7] H. Matsunaga, “Free vibration and stability of thick elastic plates subjected to in-plane forces”, International Journal of Solids and Structures, 31, 3113-3124, 1994.

[8] R.C. Batra, S. Aimmanee, “Vibrations of thick isotropic plates with higher order shear and normal deformable plate theories”, Computers and Structures, 83, 934-955, 2005.

[9] A.W. Leissa, “Vibration of plates”, NASA SP-160, Office of Technology Utilization, Washington, 1969.

[10] Y. Narita, A.W. Leissa, “Flexural vibrations of free circular plates elastically constrained along parts of the edge”, International Journal of Solids and Structures, 17, 83-92, 1981.

[11] M. Amabili, R. Pierandrei, G. Frosali, “Analysis of vibrating circular plates having non-uniform constraints using the modal properties of free-edge plates: application to bolted plates”, Journal of Sound and Vibration, 206, 23-38, 1997.

[12] T. Irie, G. Yamada, K. Takagi, “Natural frequencies of circular plates”, Journal of Applied Mechanics, 47, 652-655, 1980.

[13] K.M. Liew, J.B. Han, Z.M. Xiao, “Vibration analysis of circular Mindlin plates using the differential quadrature method”, Journal of Sound and Vibration, 205, 617-630, 1997.

[14] J.R. Hutchinson, “Vibration of thick free circular plates, exact versus approximate solutions”, Journal of Applied Mechanics, 51, 581-585, 1984.

[15] J. So, A.W. Leissa, “Three-dimensional vibrations of thick circular and annular plates”, Journal of Sound and Vibration, 209, 15-41, 1998.
[16] K.M. Liew, B. Yang, “Elasticity solutions for free vibrations of annular plates from three-dimensional analysis”, International Journal of Solids and Structures, 37, 7689-7702, 2000.
[17] D. Zhou, F.T.K. Au, Y.K. Cheung, S.H. Lo, “Three-dimensional vibration analysis of circular and annular plates via the Chebyshev-Ritz method”, International Journal of Solids and Structures, 40, 3089-3105, 2003.
[18] Sh. Hosseini-Hashemi, H. Rokni Damavandi Taher, M. Omidi, “3-D free vibration analysis of annular plates on Pasternak elastic foundation via p-Ritz method”, Journal of Sound and Vibration, 311, 1114-1140, 2008.
[19] L.W. Chen, J.R. Hwang, “Vibrations of initially stressed thick circular and annular plates based on a high-order plate theory”, Journal of Sound and Vibration, 122, 79-95, 1988.
[20] Sh. Hosseini-Hashemi, M. Es’haghi, H. Rokni Damavandi Taher, M. Fadaie, “Exact closed-form frequency equations for thick circular plates using a third-order shear deformation theory”, Journal of Sound and Vibration, 329, 3382-3396, 2010.
[21] H. Bisadi, M. Es’haghi, H. Rokni Damavandi Taher, M. Ilkhani, “Benchmark solution for transverse vibration of annular Reddy plates”, International Journal of Mechanical Sciences, 56, 35-49, 2012.
[22] L. Dozio, E. Carrera, “A variable kinematic Ritz formulation for vibration study of quadrilateral plates with arbitrary thickness”, Journal of Sound and Vibration, 18-19, 4611-4632, 2011.
[23] E. Carrera, “A class of two dimensional theories for multilayered plates analysis”, Atti Accademia delle Scienze di Torino, Memorie Scienze Fisiche, 49-87, 1995.

Appendix A

By introducing the following thickness integrals

$$E_{\tau s} = \int_{-h/2}^{+h/2} F_\tau(z) F_s(z) \mathrm{d}z \qquad E_{\tau s_{,z}} = \int_{-h/2}^{+h/2} F_\tau(z) \frac{\mathrm{d}F_s(z)}{\mathrm{d}z} \mathrm{d}z$$

$$E_{\tau_{,z} s} = \int_{-h/2}^{+h/2} \frac{\mathrm{d}F_\tau(z)}{\mathrm{d}z} F_s(z) \mathrm{d}z \qquad E_{\tau_{,z} s_{,z}} = \int_{-h/2}^{+h/2} \frac{\mathrm{d}F_\tau(z)}{\mathrm{d}z} \frac{\mathrm{d}F_s(z)}{\mathrm{d}z} \mathrm{d}z$$

the matrices $\mathbf{Z}_{\tau s}^{\mathrm{pp}}, \ldots, \mathbf{Z}_{\tau s}^{\rho}$ in Eqs. (25) and (26) are defined as follows:

$$
\begin{aligned}
\mathbf{Z}_{\tau s}^{\mathrm{pp}} &= E_{\tau s}\mathbf{C}_{\mathrm{pp}} & \mathbf{Z}_{\tau s}^{\mathrm{pn}} &= E_{\tau s}\mathbf{C}_{\mathrm{pn}} \\
\mathbf{Z}_{\tau s}^{\mathrm{np}} &= E_{\tau s}\mathbf{C}_{\mathrm{np}} & \mathbf{Z}_{\tau s}^{\mathrm{nn}} &= E_{\tau s}\mathbf{C}_{\mathrm{nn}} \\
\mathbf{Z}_{\tau s_{,z}}^{\mathrm{pn}} &= E_{\tau s_{,z}}\mathbf{C}_{\mathrm{pn}} & \mathbf{Z}_{\tau s_{,z}}^{\mathrm{nn}} &= E_{\tau s_{,z}}\mathbf{C}_{\mathrm{nn}} \\
\mathbf{Z}_{\tau_{,z} s}^{\mathrm{np}} &= E_{\tau_{,z} s}\mathbf{C}_{\mathrm{np}} & \mathbf{Z}_{\tau_{,z} s}^{\mathrm{nn}} &= E_{\tau_{,z} s}\mathbf{C}_{\mathrm{nn}} \\
\mathbf{Z}_{\tau_{,z} s_{,z}}^{\mathrm{nn}} &= E_{\tau_{,z} s_{,z}}\mathbf{C}_{\mathrm{nn}} & \mathbf{Z}_{\tau s}^{\rho} &= E_{\tau s}\rho
\end{aligned}
$$

Appendix B

After introducing the quantities

$$\Gamma_c = \int_0^{2\pi} \cos^2(n\theta)\mathrm{d}\theta \qquad (n = 0, 1, 2, \ldots)$$

$$\Gamma_s = \int_0^{2\pi} \sin^2(n\theta)\mathrm{d}\theta \qquad (n = 0, 1, 2, \ldots)$$

and defining the following integrals

$$I_{\alpha\beta}^{abc} = \int_{-1}^{+1} \frac{\mathrm{d}^a \phi_{\alpha\tau i}}{\mathrm{d}\xi^a} \frac{\mathrm{d}^b \phi_{\beta s j}}{\mathrm{d}\xi^b} (\xi + \delta)^c \, \mathrm{d}\xi$$

the elements of the stiffness fundamental nucleus $\mathbf{K}_{\tau s i j}$ can be explicitly written as follows:

$$
\begin{aligned}
K_{\tau s i j}(1,1) &= E_{\tau s} C_{11}\, \Gamma_c I_{\xi\xi}^{111} + E_{\tau s} C_{22}\, \Gamma_c I_{\xi\xi}^{00-1} + E_{\tau s} C_{12}\, \Gamma_c \left(I_{\xi\xi}^{100} + I_{\xi\xi}^{010} \right) \\
&\quad + E_{\tau s} C_{66}\, n^2\, \Gamma_s I_{\xi\xi}^{00-1} + E_{\tau_{,z} s_{,z}} C_{55}\, \gamma^2\, \Gamma_c I_{\xi\xi}^{001} \\
K_{\tau s i j}(1,2) &= E_{\tau s} C_{12}\, n\, \Gamma_c I_{\xi\theta}^{100} + E_{\tau s} C_{22}\, n\, \Gamma_c I_{\xi\theta}^{00-1} + E_{\tau s} C_{66}\, n\, \Gamma_s \left(I_{\xi\theta}^{00-1} - I_{\xi\theta}^{010} \right) \\
K_{\tau s i j}(1,3) &= E_{\tau s_{,z}} C_{13}\, \gamma\, \Gamma_c I_{\xi z}^{101} + E_{\tau s_{,z}} C_{23}\, \gamma\, \Gamma_c I_{\xi z}^{000} + E_{\tau_{,z} s} C_{55}\, \gamma\, \Gamma_c I_{\xi z}^{011} \\
K_{\tau s i j}(2,1) &= E_{\tau s} C_{12}\, n\, \Gamma_c I_{\theta\xi}^{010} + E_{\tau s} C_{22}\, n\, \Gamma_c I_{\theta\xi}^{00-1} + E_{\tau s} C_{66}\, n\, \Gamma_s \left(I_{\theta\xi}^{00-1} - I_{\theta\xi}^{100} \right) \\
K_{\tau s i j}(2,2) &= E_{\tau s} C_{22}\, n^2\, \Gamma_c I_{\theta\theta}^{00-1} + E_{\tau s} C_{66}\, \Gamma_s \left(I_{\theta\theta}^{111} - I_{\theta\theta}^{100} - I_{\theta\theta}^{010} + I_{\theta\theta}^{00-1} \right) \\
&\quad + E_{\tau_{,z} s_{,z}} C_{44}\, \gamma^2\, \Gamma_s I_{\theta\theta}^{001} \\
K_{\tau s i j}(2,3) &= E_{\tau s_{,z}} C_{23}\, n\gamma\, \Gamma_c I_{\theta z}^{000} - E_{\tau_{,z} s} C_{44}\, n\gamma\, \Gamma_s I_{\theta z}^{000} \\
K_{\tau s i j}(3,1) &= E_{\tau_{,z} s} C_{13}\, \gamma\, \Gamma_c I_{z\xi}^{011} + E_{\tau_{,z} s} C_{23}\, \gamma\, \Gamma_c I_{z\xi}^{000} + E_{\tau s_{,z}} C_{55}\, \gamma\, \Gamma_c I_{z\xi}^{101} \\
K_{\tau s i j}(3,2) &= E_{\tau_{,z} s} C_{23}\, n\gamma\, \Gamma_c I_{z\theta}^{000} - E_{\tau s_{,z}} C_{44}\, n\gamma\, \Gamma_s I_{z\theta}^{000} \\
K_{\tau s i j}(3,3) &= E_{\tau s} C_{55}\, \Gamma_c I_{zz}^{111} + E_{\tau s} C_{44}\, n^2\, \Gamma_s I_{zz}^{00-1} + E_{\tau_{,z} s_{,z}} C_{33}\, \gamma^2\, \Gamma_c I_{zz}^{001}
\end{aligned}
$$

The non-null elements of the mass fundamental nucleus $\mathbf{M}_{\tau sij}$ are given by

$$\begin{aligned} M_{\tau sij}(1,1) &= E_{\tau s}\rho\,\gamma^2\,\Gamma_c I_{\xi\xi}^{001} \\ M_{\tau sij}(2,2) &= E_{\tau s}\rho\,\gamma^2\,\Gamma_s I_{\theta\theta}^{001} \\ M_{\tau sij}(3,3) &= E_{\tau s}\rho\,\gamma^2\,\Gamma_c I_{zz}^{001} \end{aligned}$$

By setting $n = 0$ in the above equations, axisymmetric modes are obtained. Note that, in this case, $K_{\tau sij}(1,2) = K_{\tau sij}(2,1) = K_{\tau sij}(2,2) = K_{\tau sij}(2,3) = K_{\tau sij}(3,2) = 0$ and $M_{\tau sij}(2,2) = 0$.

In the case of torsional modes, the circumferential is once again null, but now Γ_c is replaced by Γ_s and conversely. Therefore, the only non-zero terms are the following:

$$K_{\tau sij} = E_{\tau s} C_{66}\,\Gamma_c\left(I_{\theta\theta}^{111} - I_{\theta\theta}^{100} - I_{\theta\theta}^{010} + I_{\theta\theta}^{00-1}\right) + E_{\tau_{,z} s_{,z}} C_{44}\,\gamma^2\,\Gamma_c I_{\theta\theta}^{001}$$

$$M_{\tau sij} = E_{\tau s}\rho\,\gamma^2\,\Gamma_c I_{\theta\theta}^{001}$$